Table 1 Grain yield, weather and grain growth observations for the three wheat crops

Year	Dry matter grain yield* ($g\ m^{-2}$)	Anthesis until cessation of grain growth: Duration (d)	Actual evaporation [E_a] ($mm\ d^{-1}$)	Potential evaporation [E_p] ($mm\ d^{-1}$)	E_a/E_p	During linear grain growth: Mean air temperature (°C)	Mean maximum air temperature (°C)	Mean grain growth rate [R_g] ($mg\ d^{-1}$)	Grain growth duration [D_g] (d)	Final mean weight per grain (mg)
1974	495 (46)	45	3.0	3.0	1.00	14.9	19.5	1.41	32.9	52.2
1975	535 (51)	38	2.0	3.4	0.59	16.8	21.6	1.76	25.2	50.3
1976	340 (32)	25	2.1	4.6	0.46	20.7	28.5	2.11	14.5	36.6

*Farm yields in cwt $acre^{-1}$ at 15% moisture are shown in parentheses.

for the 3 yr. Table 1 gives the relevant values of the variables of equation (1). Compared with 1974 the warmer, drier weather of 1975 was associated with a slightly faster R_g but this was offset by a decrease in D_g so that $\overline{W}_g(f)$ was close to 50 mg in both seasons, a typical figure for Maris Huntsman[10]. In 1976 very dry weather and exceptionally high temperatures were associated with very fast R_g (Table 1). But this was more than offset by a sharp decrease in D_g so that $\overline{W}_g(f)$ was only 37 mg.

Changes of plant dry weight after anthesis must be examined in greater detail to establish the reason for the extremely short D_g in 1976.

It is convenient to distinguish two sources of assimilate supply for grain growth: photosynthesis after anthesis, and translocation of materials assimilated before anthesis and temporarily stored before moving to the grain. As a first step in assessing the importance of these two sources, increase in grain weight from anthesis to final harvest (ΔW_g) can be expressed as

$$\Delta W_g = \Delta W_t - \Delta W_s$$

where ΔW_t is the increase in total crop weight, and ΔW_s is the increase in weight of plant parts other than the grain between anthesis and harvest[5]. By far the largest proportion of ΔW_s consists of the stem and for brevity this term is referred to as stem weight. In Table 2, which shows the relevant crop dry weight changes, $-\Delta W_s/\Delta W_g$ is the fraction of final grain weight apparently derived from translocation of materials assimilated before anthesis. Even in 1974, this fraction (0.35) was much larger than the maximum of about 0.20 expected for wheat[11]. In 1975 and 1976, however, when production of dry matter after anthesis was smaller still in relation to the requirements for grain growth, the contribution of translocated materials to grain yield was much greater. This increased movement of materials from stem to grain when conditions during grain filling are adverse for photosynthesis lends support to the concept of "compensatory translocation"[5]. The small value of $\overline{W}_g(f)$ which occurred in 1976 in spite of considerable translocation of material from the stem raises two questions: is there a limit to the amount of dry matter that can be supplied to the grain by compensatory translocation; was this limit reached or exceeded in 1976?

The extent of translocation may ultimately be limited by the need to retain sufficient dry matter in the stems to support the ears. In 1976, however, supporting tissue per grain was considerably greater than in 1975 (Table 2). Thus it seems that shortage of assimilate did not limit final grain weight by curtailing the duration of grain growth. There are two other possible reasons why grain growth stopped: either the transport system to the growing grain was inadequate or starch synthesis stopped prematurely. Studies of translocation during wheat grain growth show little effect of water stress[12], but there is evidence that a fall in the synthetic capacity of the endosperm causes grain growth to stop[13]. In 1975 and 1976, the duration of starch synthesis could have been limited either by the effect of drought on plant water status or by abnormally high ear temperatures. The relative importance of these two correlated factors cannot be determined from our measurements, but related work in controlled environments indicates that temperature rather than water stress stops grain growth prematurely[14–16].

Table 2 Crop weight measurements

Year	Increase in weight (gm^{-2}) between anthesis and harvest: Grain [ΔW_g]	Total [ΔW_t]	Stem [ΔW_s]	$-\Delta W_s/\Delta W_g$	Stem weight per grain (mg)
1974	495	322	−173	0.35	65
1975	532	228	−304	0.57	54
1976	341	149	−192	0.56	63

These results illustrate the potential importance of translocation of material assimilated before anthesis to grain growth when current photosynthesis is limited by an adverse environment. They also establish the usefulness of treating grain growth as a linear process and expressing final weight per grain as a product of a growth rate and duration. If cereals are to yield well in regions where drought and high temperatures during grain filling are frequent, varieties must be bred which not only increase the rate but also sustain the duration of grain growth. Such characteristics would maximise the assimilate to be harvested in the nutritionally valuable fraction of the crop.

We thank Dr M. McGowan for the measurements of crop evaporation, the Royal Society (J.N.G.) and the ARC for financial support.

J. N. GALLAGHER
P. V. BISCOE
B. HUNTER

University of Nottingham,
School of Agriculture,
Sutton Bonington, Loughborough LE12 5RD, UK

Received September 21; accepted October 20, 1976.

1 *Agrometeorology of the Wheat Crop*, Symp. No. 369 (World Meteorological Organisation, Geneva, 1974).
2 Stone, J. F. (ed.), *Plant Modification for more Efficient Water Use, Agric. Meteorol.*, Special Issue (1974).
3 Gallagher, J. N., Biscoe, P. V., and Scott, R. K., *J. appl. Ecol.*, 13, 563–583 (1976).
4 Riggs, T. R., and Gothard, P. G., *J. agric. Sci.*, 86, 603–608 (1976).
5 Gallagher, J. N., Biscoe, P. V., and Scott, R. K., *J. appl. Ecol.*, 12, 319–336 (1975).
6 McGowan, M., in *Proc. Symp. Isotope and Radiation Techniques in Soil Physics Studies*, 435–445, (International Atomic Energy Agency, Vienna, 1974).
7 Smith, L. P., *Potential Transpiration, Tech. Bull. Minist. Agric. Fish. Fd.*, 16 (Her Majesty's Stationery Office, London, 1967).
8 Duncan, W. G., in *Crop Physiology* (edit. by Evans, L. T.), 23–50 (Cambridge University Press, London, 1975).
9 Sofield, D. I., Evans L. T., and Wardlaw I. F., *Bull. R. Soc. N.Z. 2.*, 12, 909–915 (1974).
10 Pushman, F. M., and Bingham J., *J. agric. Sci*, 85, 559–563 (1975).
11 Thorne, G. N., in *The Growth of Cereals and Grasses* (edit. by Milthorpe. F. L., and Ivins, J. D.), 88–105, (Butterworths, London, 1966).
12 Wardlaw, I. F., *Aust. J. biol. Sci.*, 22, 1–16 (1967).
13 Jenner, C. F., and Rathjen, A. J., *Aust. J. Pl. Physiol.*, 2, 311–322 (1975).
14 Asana, R. D., and Williams, F. R., *Aust. J. agric. Res.*, 16, 1–13 (1974).
15 Spiertz, J. H. J., *Neth. J. agric. Sci.*, 22, 207–220 (1974).
16 Asana, R. D., and Saini, A. D., *Physiol. Pl.*, 11, 666–674 (1958).

Predicting the course of Gompertzian growth

THE increase in volume or size with time that characterises many biological and physical systems is often well approximated retrospectively by mathematical 'growth curves'. In some cases, however, growth may be sufficiently complicated for it to be impossible to predict later portions of the growth curve if observations are limited to a few early points. We report here the development of a generalised approach to

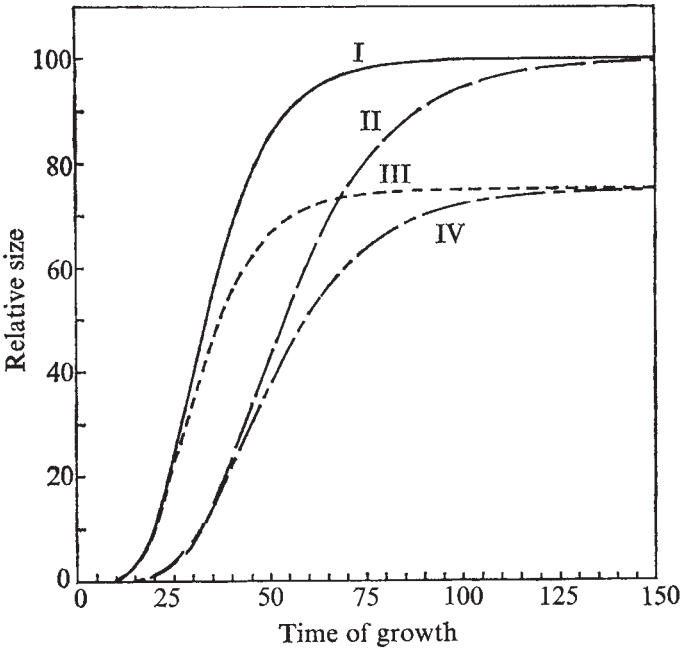

Fig. 1 Hypothetical Gompertzian curves derived by solving equation (3) with various parameters A and B as follows: Curve I, $A = 0.4$, $B = 0.4/(\ln 100)$; Curve II, $A = 0.25$, $B = 0.25/(\ln 100)$; Curve III, $A = 0.4$, $B = 0.4/(\ln 75)$; Curve IV, $A = 0.25$, $B = 0.25/(\ln 75)$. Note that the early portion of the curve reflects parameter A and the later portion of the curve reflects the ratio of A/B.

the analysis of "Gompertzian" growth which enables accurate predictions of future growth for two model tumour systems. This mathematical method may be useful clinically, and expresses a property of biological growth that may be applicable to other systems.

The growth of most experimental neoplasms[2–4], human populations[5], normal embryos[6], molluscs[7], visceral organs[8,9] and some human tumours[10] are well described by the S-shaped curves used for actuarial purposes by Benjamin Gompertz in 1825 (ref. 1). The essential distinguishing feature of Gompertzian growth (Fig. 1), is some mechanism of feedback inhibition with increasing size, resulting in decremented exponential growth that achieves a limiting size asymptotically. Unfortunately, the relatively complicated form of the Gompertzian equation has tended to limit its general applicability, often resulting in the alternative use of less satisfactory exponential[11–14], summed exponential[15], or other[16] growth models. These other models however, are rarely applicable to an entire growth history, and are therefore insufficient for the purposes of predicting later growth.

A Gompertzian function is the simultaneous solution of the two differential equations

$$dN(t)/dt = K_1 \cdot N(t) \cdot G(t) \quad (1)$$

$$dG(t)/dt = -K_2 \cdot G(t) \quad (2)$$

where K_i is a constant > 0, $N(t)$ is volume at time t, and $G(t)$ is a function entirely described by equation (2). The expression $K_2 \cdot G(t)$ can be thought of as the fraction of $N(t)$ that doubles in size during the instant dt. The solution of these equations is often written in the form

$$N(t) = N(0) \cdot \exp[(K_1/K_2) \cdot G(0) \cdot \{1 - \exp(-K_2 \cdot t)\}]$$

Since

$$G(t) = G(0) \cdot \exp(-K_2 \cdot t) = (K_2/K_1) \cdot \ln[N(\infty)/N(t)]$$

where $N(\infty) = \lim_{t \to \infty} N(t)$, an alternative form of equation (1) is

$$dN(t)/dt = K_2 \cdot N(t) \cdot \ln[N(\infty)/N(t)]$$
$$= A \cdot N(t) - B \cdot N(t) \cdot \ln[N(t)] \quad (3)$$

where $B = K_2$ and $A = K_2 \cdot \ln[N(\infty)]$. The dependence of the pattern of growth of $N(t)$ on A and B is illustrated in Fig. 1. For a given $N(0)$, when A is constant, the early phase of growth (often referred to loosely as the exponential phase) is similar in spite of different values of B. Also, when A/B is constant, the later phase of growth (the plateau phase) is similar in spite of different values of A. Were A and B unrelated, knowledge of the early phase of growth of a particular system (tumour, organ, embryo, or population) would not enable an accurate prediction of the later phase, as the value of A, but not A/B, could be estimated from the early growth pattern. Similarly, measurements of late growth would provide an estimate of A/B but not A. On the other hand, if it were possible to estimate B from A, the entire growth pattern of an individual system would be predictable on the basis of measurements early in its growth history.

For eight cases of B-16 melanoma in BDF_1 mice and ten cases of transplantable mammary carcinoma 13672 in Fischer 344 rats, measurements of length (L) and width (W) were obtained during unperturbed growth from the time of transplant until the death of the host or the occurrence of tumour ulceration. Approximate tumour volumes (V) were calculated as the volume of revolution of an ellipse by the formula

$$V = (\pi/6) L W^2$$

The growth of these tumours (Fig. 2) demonstrates the variability typical of malignant proliferation.

For each tumour, the solution of equation (3) was fit using the method of least squares to the curve of volume as a function of time of growth starting from the hypothetical volume of a single cell. Examples of curves fitted to data for each tumour type are illustrated in Fig. 3. Each curve fit yields the two parameters, A and B, that completely describe the growth pattern

Fig. 2 The volume of eight examples of B-16 melanoma (——) and ten examples of 13762 carcinoma (– – –) plotted as a function of time from initiation of growth. The volume scale is arithmetic. The variability in growth pattern typical of neoplastic proliferation is evident.

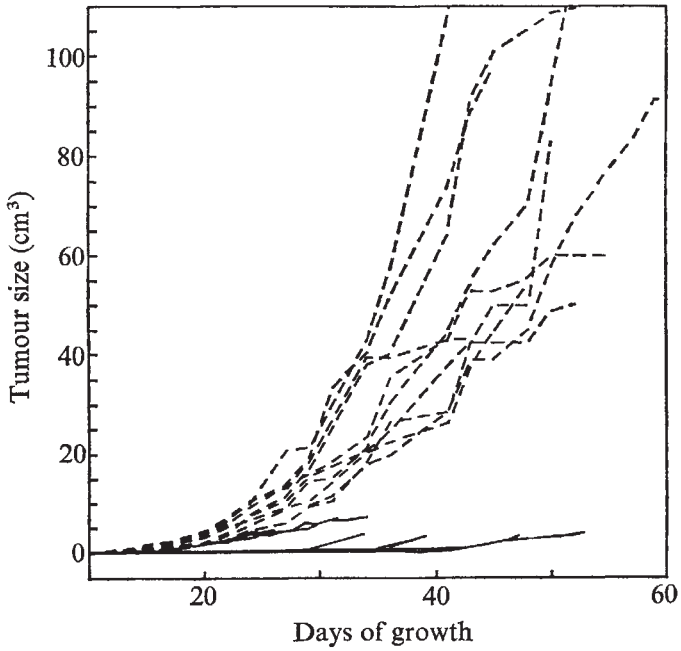

for that tumour. As seen in Fig. 4, when $\exp(A)$ is plotted against $\ln(B)$ for all individuals of each tumour type, the relationship is found to be linear with correlation coefficients of 0.99 for B-16 melanoma ($P < 0.0000002$) and 0.96 for the rat carcinoma ($P < 0.000006$). This high degree of correlation between the transforms of A and B allows, for these experimental tumours, the accurate prediction of B on the basis of an estimate of A made from measurement of the early phase of growth of an individual tumour. Equation (3) may therefore be written

$$dN(t)/dt = A \cdot N(t) - \exp[(\exp\{A\} - n)/m] \cdot N(t) \cdot \ln[N(t)] \quad (4)$$

a Gompertzian equation in one variable, A, with constants n, m, and $N(0)$ (the volume of a single cell) specific for a particular tumour type.

Having determined empirically the constants n and m for a tumour type, the total growth curve for an individual tumour of that type can be predicted accurately from a few early measurements of volume. In Fig. 3, for example, the solution of equation (4) was fit to three early measurements of a tumour not used to derive the above relationship between A and B. The prediction obtained is seen to match closely the actual volumes observed later in the growth of the tumour.

The ability to predict the later growth pattern of an individual tumour on the basis of early growth measurements should have widespread applicability, not only in the design of experimental anti-cancer therapy, but in the diagnosis and prognosis of human tumours as well. For example, the response of an individual cancer to treatment could be expressed in terms of deviation from ideal unperturbed growth as predicted from measurements taken before therapy. This precise method of monitoring therapy has obvious advantages over parameters presently in use, such as rate of complete or partial remission or average tumour size at some arbitrary point after therapy. These conventional endpoints are inapplicable to individual tumours, are potentially biased by drug or other non-tumour deaths, and may underestimate the influence of weakly effective forms of therapy which may nevertheless be potentially useful in combinations.

Fig. 3 Examples of equation (3) fit to data for B-16 melanoma (□) and 13762 rat carcinoma (△). The volume scale is logarithmic. The dashed lines represent the fitted curves. Paired constants (A, B) derived from several such curve fits are plotted in Fig. 4. The points marked 0 are three early volume measurements for an individual 13762 rat carcinoma not used to derive the constants n and m (see text). Equation (4) was fit to these three points using constants n and m from Fig. 4; the resulting solid line is seen to predict accurately the later growth measurements (●) for that tumour; measurements unknown at the time of curve fitting.

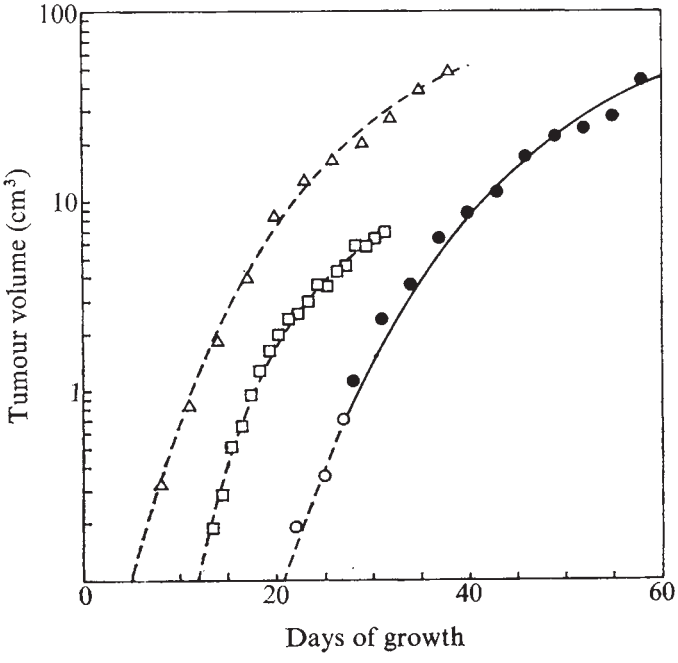

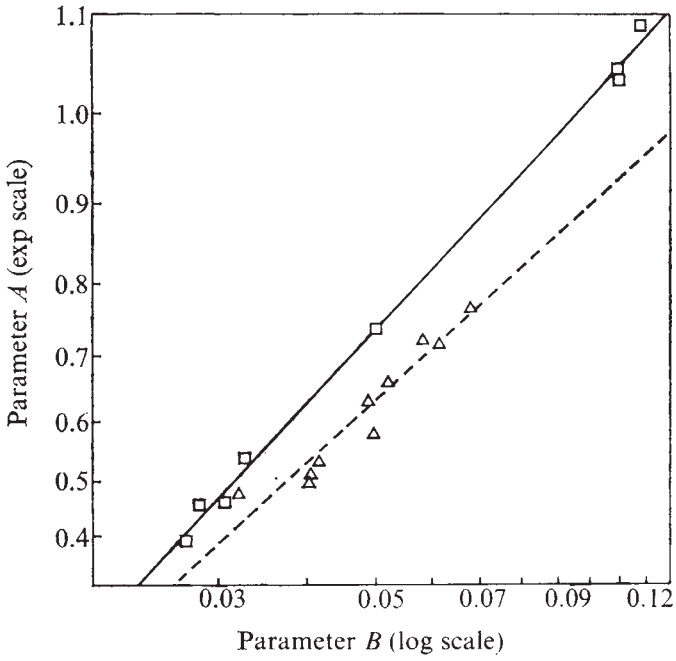

Fig. 4 Correlation between $\exp(A)$ and $\ln(B)$ for B-16 melanoma (□) and 13762 rat carcinoma (△). The points represent pairs of parameters (A, B) determined from curve fits as illustrated in Fig. 3; the solid lines represent the regression equation $\exp(A) = m.\ln(B) + n$, with the following values of m, n, respectively: B-16 melanoma, 0.9645 and 4.980; 13762 carcinoma, 0.8176 and 4.334.

For these two experimental tumours the methods described here reveal a remarkable orderliness of growth that tends to dispel the concept of cancer as a wild and uncontrolled phenomenon. We may expect that the growth of non-neoplastic tissues (for example, gut epithelium, bone marrow and regenerating liver) would be at least as orderly as that of these two malignancies. Results obtained by applying these methods to normal tissues will be reported later. These mathematical methods may also be applied to the growth of mammalian or bacterial cells in culture, with obvious use in the monitoring of growth inhibitory influences (such as hormones and antibiotics). We also plan to describe the applications of these methods to other tumour types, paying particular attention to the description and prediction of the response of malignancies to single and multiple agent therapies.

LARRY NORTON
RICHARD SIMON
Biostatistics and Data Management Section,
Clinical Oncology Program,
Division of Cancer Treatment

HARMAR D. BRERETON
Radiation Oncology Program,
Division of Cancer Treatment,
National Cancer Institute,
Bethesda, Maryland 20014

ARTHUR E. BOGDEN
Mason Research Institute,
Worcester, Massachusetts

Received June 2; accepted October 12, 1976.

1 Gompertz, B., *Phil. Trans. R. Soc.*, **115**, 513–585 (1825).
2 Laird, A. K., *Br. J. Cancer*, **18**, 490–502 (1964).
3 McCredie, J. A., Inch, W. R., Kruuv, J., and Watson, T. A., *Growth*, **29**, 331–347 (1965).
4 Simpson-Herren, L., and Lloyd, H. H., *Cancer Chemother. Rep.*, **54**, 143–174 (1970).
5 Shryock, H. S., and Siegel, J. S., *The Methods and Materials of Demography* (US Government Printing Office, Washington, DC, 1973).

6 Laird, A. K., Tyler, S. A., and Barton, A. D., *Growth*, **29**, 233–248 (1965).
7 Weymouth, F. W., McMillin, H. C., and Rich, W. H., *J. exp. Biol.*, **8**, 228–249 (1931).
8 Laird, A. K., *Growth*, **29**, 249–263 (1965).
9 Laird, A. K., *Natn. Cancer Inst. Monogr.*, **30**, 15–28 (1969).
10 Sullivan, P. W., and Salmon, S. E., *J. clin. Invest.*, **51**, 1697–1708 (1972).
11 Collins, V. P., Loeffler, K., and Tivey, H., *Am. J. Roentgenol.*, **76**, 988–1000 (1956).
12 Skipper, H. E., Schabel, F. M., Jr, and Wilcox, W. S., *Cancer Chemother. Rep.*, **35**, 1–111 (1964).
13 Wilcox, W. S., Griswold, D. P., and Laster, W. R., Jr, *Cancer Chemother. Rep.*, **47**, 27–39 (1965).
14 Duchatellier, M., and Israel, L., *Eur. J. Cancer*, **7**, 545–549 (1971).
15 Looney, W. B., Trefil, J. S., Schaffner, J. C., Kovacs, C. J., and Hopkins, H. A., *Proc. natn. Acad. Sci. U.S.A.*, **72**, 2662–2666 (1975).
16 Baserga, R., *Cancer Res.*, **25**, 581–595 (1965).

Significance of cell shape in tissue architecture

STIMULI passing to a cell within solid tissue are modulated by the cellular environment. Control mechanisms must therefore involve both humoral influences and the architecture of the cellular microenvironment. Epidermis suffers a constant loss of surface cells which are replaced by basal cells which have differentiated during migration to the surface. In mouse ear and dorsum, the path of this migration can be observed as precisely defined columns of cells[1] which are in tetrakaidecahedral[2] form (Fig. 1) as in the rigid cell walls of plant tissues[3]. Recent studies[3,4] have suggested that maintenance of this system of 'dynamic orderedness' may be explained by reference to its physical geometry, and minimal surface packing configurations. In this paper we discuss some of the consequences of this view of tissue architecture.

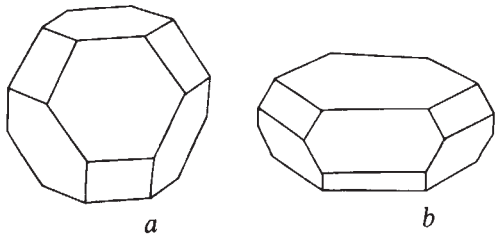

Fig. 1 *a*, Line drawing of an orthic tetrakaidecahedron. This 14-sided figure consists of six equal opposite quadrilateral faces and eight equal and opposite hexagons. Each quadrilateral face is bounded by four hexagons and each hexagonal face by three hexagons and three quadrilaterals. *b*, When compressed about a pair of hexagonal faces the shape assumed will become predominantly hexagonal, with the remaining 12 faces becoming hexagonal and quadrilateral facets around the edges.

The ordered epidermis of mouse ear or dorsum shows keratinised squames piled in columns and presenting a characteristic hexagonal patterning[1,5], when viewed from the surface (Fig. 2). It is clear from the flattened nature of these cells that if they are tetrakaidecahedral, then the orthic form of the tetrakaidecahedron has become distorted to a flattened version (Fig. 1), in which the flattening has resulted in an increase in area of a pair of the hexagonal faces, reducing the remaining 12 faces to alternate quadrilateral and hexagonal facets around the edges. These facets may be observed in the scanning electron microscope particularly if some of the outer squames are removed (Fig. 2).

From the density packing configuration of either orthic or flattened tetrakaidecahedra, there is only one way in which these shapes can be assembled. This results in a columnar organisation in which the top 'cell ' of the central column, of any group selected, occupies a position at the lowest or highest level, relative to the surrounding six adjacent columns which are

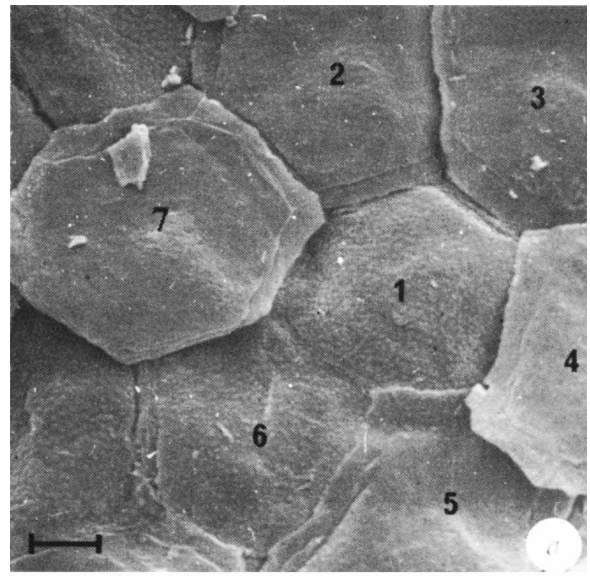

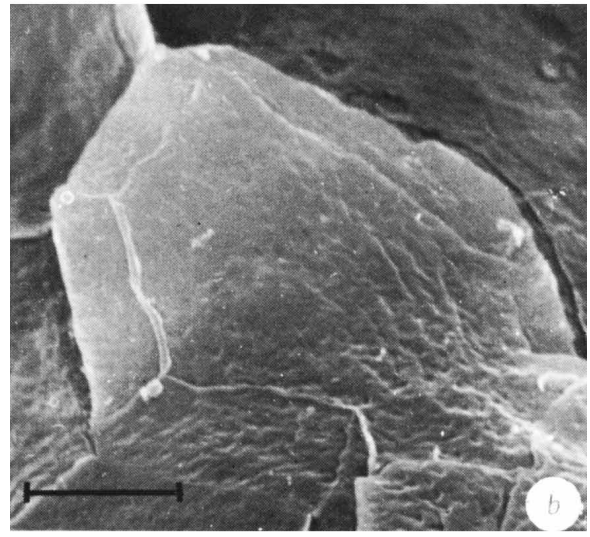

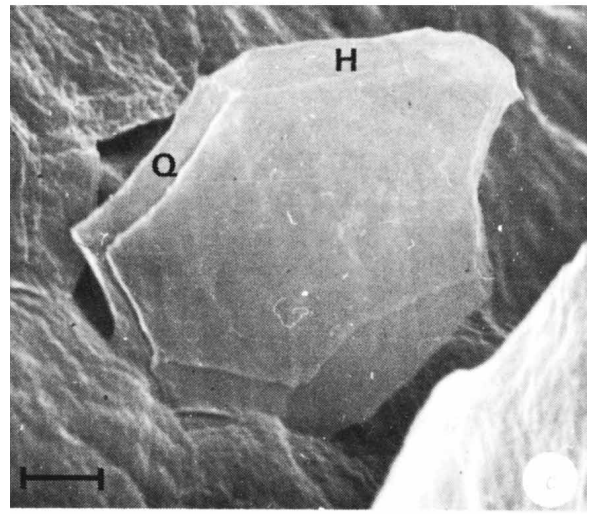

Fig. 2 *a*, Area of mouse ear epidermis showing a central hexagonal squame (1) and its six surrounding neighbours (2–7). Squame 1 is overlapped on all edges, and so cannot desquamate until all the surrounding cells (2–7) have done so, whereas squame 7 has all edges free and is able to desquamate. The region of overlap (previously covered by the last squame in the central pile) and the interdigitating facets are visible at the edges of the surrounding squames. At this advanced stage of flattening that occurs close to the surface, the facets at the squame edge have largely lost their characteristic alternate hexagonal and quadrilateral appearance because of the overall distortion, but still provide evidence of the tetrakaidecahedral form adopted in the less keratinised and more plastic regions of the granular layer. Scale bar: 5 μM. *b*, *c*, Cells exposed from some distance below the surface showing clearly the facets at the edge providing the interdigitating regions. In some cells (*c*) a close approximation to the alternate hexagon (H) and quadrilateral (Q) faceting seen in the true geometric tetrakaidecahedron (Fig. 1*b*) is apparent. Scale bars: 5 μM.